processes

MDPI

*Article*

# Experimental Study of Plugging Agent Particle Size and Concentration on Temporary Plugging Fracturing in Shale Formation

**Feng Yang [1], Qin Qian [1], Mingjing Lu [1], Wenjun He [1], Anhai Zhong [1], Zilin Zhang [1], Danyang Zhu [2] and Yushi Zou [2,*]**

[1] Research Institute of Petroleum Engineering, Sinopec Shengli Oilfield Company, Dongying 257000, China; yangfeng716.slyt@sinopec.com (F.Y.)
[2] State Key Laboratory of Petroleum Resources and Prospecting, China University of Petroleum, Beijing 102249, China
* Correspondence: zouyushi@126.com

**Abstract:** During the temporary plugging fracturing (TPF) process, the pressure response and pumping behavior significantly differ from those observed during conventional fracturing fluid pumping. Once the temporary plugging agent (TPA) forms a plug, subsequent fracture initiation and propagation become more intricate due to the influence of the TPA and early fractures. Factors such as concentration, particle size, and ratio of the TPA notably affect the effectiveness of TPF. This study employs a true triaxial hydraulic fracturing simulation system to conduct TPF experiments with varying particle size combinations and concentrations at both in-fracture and in-stage locations. The impact of different TPA parameters on the plugging effectiveness is assessed by analyzing the morphology of the induced fractures and the characteristics of pressure curves post experiment. Results indicate that combining dfferent particle sizes enhances plugging effectiveness, with a combination of smaller and larger particles exhibiting superior plugging effectiveness, resulting in a pressure increase of over 25.9%. As the concentration of the TPA increases, the plugging fracture pressure rises, accompanied by rapid pressure response and significant plugging effects, leading to more complex fracture morphology. For shale reservoirs, the density of bedding planes (BPs) influences the morphology and width of conventional hydraulic fractures, thereby affecting the effectiveness of subsequent refracturing. Rock samples with a relatively low BP density demonstrate effective plugging initiation both in-fracture and in-stage, facilitating the formation of complex fracture networks. Conversely, specimens with a relatively high BP density exhibit superior plugging effectiveness in-stage compared to in-fracture plugging.

**Keywords:** shale; temporary plugging fracturing; fracture morphology



**Citation:** Yang, F.; Qian, Q.; Lu, M.; He, W.; Zhong, A.; Zhang, Z.; Zhu, D.; Zou, Y. Experimental Study of Plugging Agent Particle Size and Concentration on Temporary Plugging Fracturing in Shale Formation. *Processes* **2024**, *12*, 1049. https://doi.org/10.3390/pr12061049

Academic Editor: Qibin Li

Received: 14 April 2024
Revised: 6 May 2024
Accepted: 17 May 2024
Published: 21 May 2024



## 1. Introduction

Horizontal well development in shale reservoirs often employs multi-cluster perforation, which offers advantages such as a large treatment volume, high efficiency, and low cost. However, it also entails stress interference among densely clustered fractures, which can lead to uneven propagation. The "dual-plugging" technique, involving both in-fracture and in-stage plugging, utilizes TPA to obstruct fracture tips and perforation clusters, inducing redirection of fracture tips and generating new cluster fractures near plugged perforation clusters. This technique represents a significant avenue for enhancing fractures' balanced extension and complexity, holding technical potential in shale oil development.

Numerous scholars have researched the mechanisms and experimental methods of fracture plugging. For the most common particle plugging agents, there are two mechanisms: one involves using fine particles (or powder) to form a filter cake on the fracture wall, thereby reducing permeability; the other consists of a combination of multiple particle sizes, where larger particles bridge within the fracture, while smaller particles plug the

voids between bridging particles, known as "bridging + plugging" [1,2]. The particle size of TPA in drilling fluids should be at least "one-third" of the pore diameter of the reservoir [3]. Considering the interstitial space between particles, the particle size distribution of TPA can be optimized using the "ideal packing theory" [4]. Since fractures are filled with proppants, the size of TPA should be based on the median particle size of the proppants [5]. Typical combinations of TPA have a bimodal distribution [6]. For far-field plugging, a combination of medium and fine particles in a 35:65 ratio can be used, while for near-wellbore plugging, larger particles should be added, comprising up to 40% of the total [7]. In experiments, plugging agents' plugging behavior with particle sizes of 20 to 30 mesh in fractures was evaluated using a core flow apparatus [8]. A large-scale visual fracture simulation device was made of organic glass to study the plugging behavior of fibers and particles within fractures [9]. The surface morphology of fractures was replicated using resin materials to create visual rough fracture models, enabling the study of plugging agents' migration and plugging behavior within rough fractures [10]. Based on triaxial hydraulic fracturing experiments, experimental studies were conducted on diversifying fractures of different sizes of exposed rock samples, focusing on fracture initiation and propagation behavior after TPA injection [11,12]. Similar experimental methods were used to study the pressure response characteristics of fiber and particle plugging agents within hydraulic fractures [13,14]. Stainless steel grooved pipes were used to simulate fractures, studying the plugging capacity of fiber and proppant mixtures, with a focus on the effects of fiber concentration, proppant size and concentration, fluid velocity, and rheology on bridging and plugging capacity [15]. An injector connected to a rectangular slot with a specific opening and equipped with a device with a filter screen at the end was designed to simulate plugging experiments, optimizing the particle size distribution of plugging agents [16]. Evaluation criteria for plugging agents include bridging pressure capacity, compactness of the plugging body, and dissolution rate of TPA. Based on these criteria, TPA formulation was optimized for wellbore and far-end plugging [17].

While numerous scholars have researched various types and properties of TPA and their plugging characteristics, current true triaxial fracturing experiments only verify the feasibility of plugging and generating new fractures. However, there has not been a systematic investigation into the pump pressure response corresponding to different plugging positions and overall fracture morphology characteristics. Therefore, based on a true triaxial hydraulic fracturing simulation system, this study conducts plugging experiments with different particle size combinations and concentrations at both in-fracture and in-stage locations. After the experiments, combined with the morphology of the fractures and pressure curve characteristics, the impact of different TPA parameters on plugging effectiveness is analyzed.

## 2. Experimental Method

### 2.1. Shale Specimens and Fracturing Equipment

The experiment utilized a true triaxial hydraulic fracturing simulation system [18] (Figure 1). The experiment simulated the natural formation of a stress environment based on the coefficient of the stress difference. Hydraulic pressure pumps and hydraulic cylinders were employed to drive the loading plates, applying triaxial stress to the rock specimens inside the core chamber. The maximum loading stress on the x, y, and z-axis was 30 MPa. Upon completion of stress loading, an air pump was used to drive a piston within the intermediate container, injecting the fracturing fluid into the pipeline. The fracturing fluid then entered the wellbore to fracture the rock specimens via a fluid injection line controlled by a six-way valve. Pressure sensors connected to the pipeline recorded real-time data of pressure changes at the wellbore.

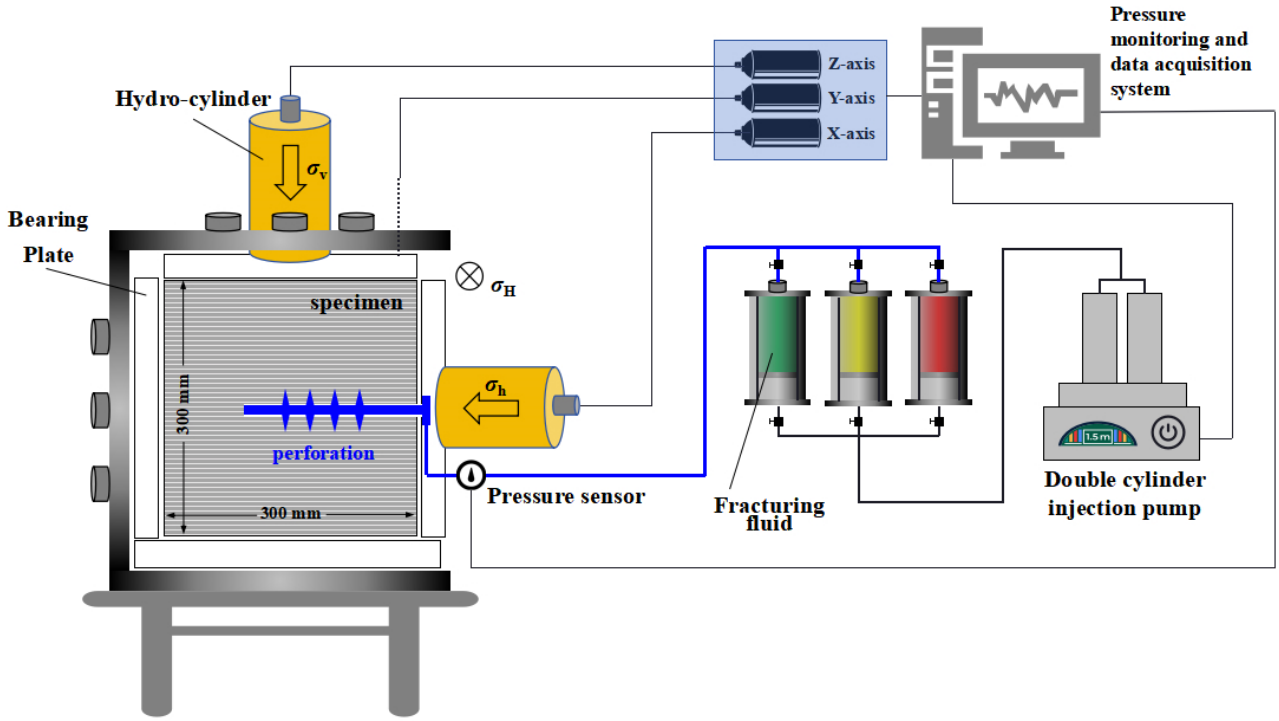


**Figure 1.** True triaxial hydraulic fracturing simulation system.

Samples were collected from outcrops in the Jiyang Depression area of the Shengli Oilfield. They were prepared into cubic specimens measuring 30 cm × 30 cm × 30 cm through cutting and grinding, with bedding surfaces parallel to the specimen ends. Small samples yielded Young's modulus ranging from 25.03 to 46.4 GPa, Poisson's ratio from 0.18 to 0.29, compressive strength from 219.1 to 406.5 MPa, and tensile strength from 4.19 to 8.34 MPa. The mechanical properties of the outcrop samples were similar to those of downhole cores from a depth of 4223 m in the same block. To simulate the completion scheme of horizontal wells with multi-cluster perforations, a blind hole with a diameter of 28 mm and a depth of 260 mm parallel to the bedding surface was drilled at the center of the specimen surface. A steel tube with an outer diameter of 27 mm and an inner diameter of 23 mm, plugged at one end and open at the other, was centrally placed in the blind hole, and high-strength epoxy resin was injected into the annulus between the blind hole and the steel tube to bond the steel tube to the specimen. A hydraulic sandblasting perforation device was used, with the perforating gun inserted into the wellbore. Perforations were made at specified depths and orientations along the wellbore wall through insertion and retraction (Figure 2). The number of perforation clusters was set to 6, with perforation spacing determined based on geometric similarity (Equation (1)) as 2.7 cm. Simulating the perforation phasing angle accurately at the current experimental scale only in the direction perpendicular to the BPs. The sandblasting perforation process was strictly controlled to ensure a uniform perforation size and depth for each perforation (4 mm in diameter, 1 cm in depth), lasting 1 min.

$$\frac{S_l}{L_l} = \beta \frac{S_f}{L_f} \tag{1}$$

where $S$ is the clusters' spacing, m; $L$ is the width of the treatment zone, m; $\beta$ (equal to 2.5) is an empirical parameter; subscript $l$ denotes experimental parameters; and subscript $f$ represents field parameters.

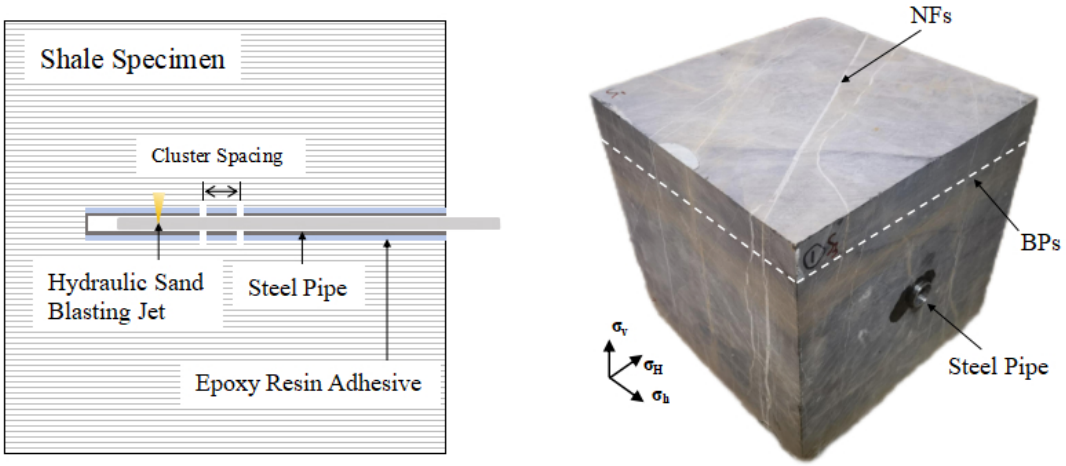


**Figure 2.** The schematic diagram of the completion method for horizontal wells with multi-cluster perforations.

### *2.2. Experimental Scheme and Procedure*

Currently, this block's on-site horizontal well fracturing injection rate ranges from 14 to 18 $m^3$/min, with cluster numbers ranging from 5 to 7 clusters. Discrepancies regarding flow rate exist between the initial and main fracturing phases. Here, considering a maximum single-cluster injection rate of 3 $m^3$/min and a fracturing fluid viscosity of 3 to 100 mPa·s (variable viscosity slickwater system), the experimental primary injection parameters were calculated using similarity criteria [19–22] (Equations (2) and (3)). Taking into account that the characteristic radius of fracture propagation in the reservoir is approximately 18.00 to 23.00 m (based on microseismic fracture monitoring half-length), whereas the characteristic radius of experimental fracture propagation is 0 to 0.3 m (half the height of the specimen), the maximum experimental injection rate was calculated to be 50 mL/min, with a fracturing fluid viscosity of 100 mPa·s. The calculation results for field and laboratory experimental parameters are presented in Table 1.

$$\mu_l = \mu_f \left[ \frac{t_{l\max}}{t_{f\max}} \left(\frac{Q_f}{Q_l}\right)^{3/2} \left(\frac{E'_f}{E'_l}\right)^{13/2} \left(\frac{K'_l}{K'_f}\right)^{9} \right]^{2/5} \tag{2}$$

where $\mu$ is the viscosity, mPa·s; $t$ is the fracture propagation time, s; $Q$ is the injection rate, $m^3$/min; $E$ is the elastic modulus of rock, GPa; $E'$ is the plane strain elastic modulus, GPa; $K'$ is the modified fracture toughness, MPa·$m^{1/2}$; subscript $l$ denotes experimental parameters; and subscript $f$ represents field parameters.

$$t_{\max} = \frac{R^{5/2}K'}{QE'} \tag{3}$$

where $R$ is the fracture propagation radius, m.

**Table 1.** The parameters of field and laboratory.

| Parameters | Field | Laboratory |
|---|---|---|
| Young's modulus (GPa) | 20–40 | 25.03–46.4 |
| Fracture characteristic radius (m) | 18–22 | 0–0.3 |
| Injection rate per single cluster ($m^3$/min) | 3–4 | 90–150 mL/min |
| Fracturing fluid viscosity (mPa·s) | 3–100 | 3–100 |

Constrained by equipment capabilities, the three-dimensional in situ stresses at corresponding reservoir depths were calculated based on log data, and the actual formation stress conditions were scaled to a laboratory scale using the shape factor $R$ [22].

$$R = \frac{\sigma_{Hl} - \sigma_{hl}}{\sigma_{Vl} - \sigma_{hl}} = \frac{\sigma_{Hf} - \sigma_{hf}}{\sigma_{Vf} - \sigma_{hf}} \quad (4)$$

where $\sigma_H$ is the maximum horizontal principal stress, MPa; $\sigma_h$ is the minimum horizontal principal stress, MPa; $\sigma_v$ is the vertical stress, MPa; subscript $l$ denotes experimental parameters; and subscript $f$ represents field parameters.

The experiment utilized maximum, minimum, and vertical principal stresses of 23 MPa, 15 MPa, and 30 MPa, respectively.

The experiment's required plugging agent particle sizes were designed based on the "one-third" bridging theory. By measuring the perforation diameters and hydraulic fracture widths displayed in the sections of early experimental specimens (Figure 3), the fracture width ranged from 0.1 to 3 mm, and the sandblasting perforation diameter near the wellbore was 4 mm. Therefore, experiments were conducted using three particle size ranges 120–80 mesh, 80–20 mesh, and 1–3 mm. Specific experimental parameters are detailed in Table 2.

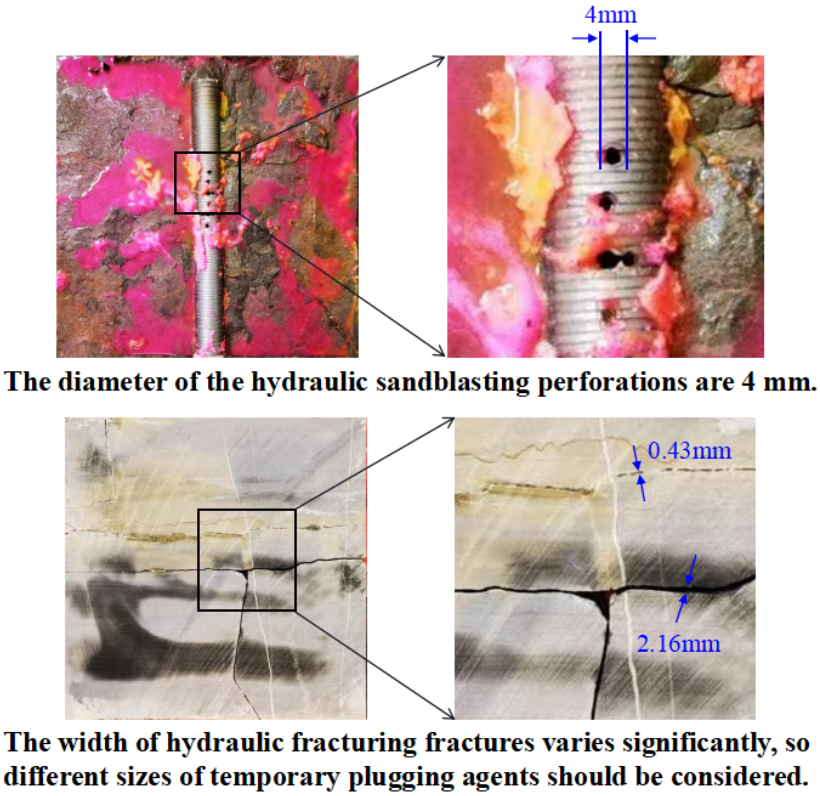


**Figure 3.** Section of earlier experimental specimens: perforation diameter and fracture width.

**Table 2.** Experimental Scheme for TPA Size and Concentration.

| NO. | In-Fracture | In-Stage |
|---|---|---|
| 1# | 50 g/L 80–120 mesh + 50 g/L 20–80 mesh, 100 g/L | 50 g 80–120 mesh + 50 g 1–3 mm, 100 g/L |
| 2# | 20–80 mesh, 100 g/L | 40 g 80–120 mesh + 40 g 20–80 mesh + 20 g 1–3 mm, 100 g/L |
| 3# | 60 g/L 80–120 mesh + 40 g/L 20–80 mesh, 100 g/L | 1–3 mm, 100 g/L |
| 4# | 50 g/L 80–120 mesh + 50 g/L 20–80 mesh, 100 g/L | 50 g 80–120 mesh + 50 g 1–3 mm, 100 g/L |
| 5# | 30 g/L 80–120 mesh + 30 g/L 20–80 mesh, 60 g/L | 30 g 80–120 mesh + 30 g 1–3 mm, 60 g/L |

Experimental procedures are as follows:

1. The pipeline was connected, and the rock specimen was placed into the core chamber of the experimental system and subjected to triaxial stress at the set value to maintain stability.
2. The fracturing pipeline was connected to the six-way valve, with the other end connected to three intermediate containers containing fracturing fluid of different colors. Container 1 contained green dye, Container 2 contained yellow dye and TPA, and Container 3 contained red dye and TPA.
3. According to the experimental process, the valves on Containers 1, 2, and 3 and their corresponding valves on the six-way valve were sequentially opened, while the remaining valves were kept closed. The injection system was activated, and fracturing fluid was continuously pumped into the wellbore at a constant rate for the hydraulic fracturing experiment. Pressure sensors recorded the changes in wellhead pressure throughout the entire process.
4. After the experiment concluded, the rock sample was moved out, and hydraulic fractures initiated during different fracturing phases were distinguished based on the coloring of the fracture surfaces, enabling analysis of the multi-fracture propagation paths near horizontal wellbore.

## 3. Experimental Results

Five sets of experiments on multi-cluster TPF in horizontal wells were conducted, corresponding to fracture morphology and pressure curves, as shown in Figure 4.

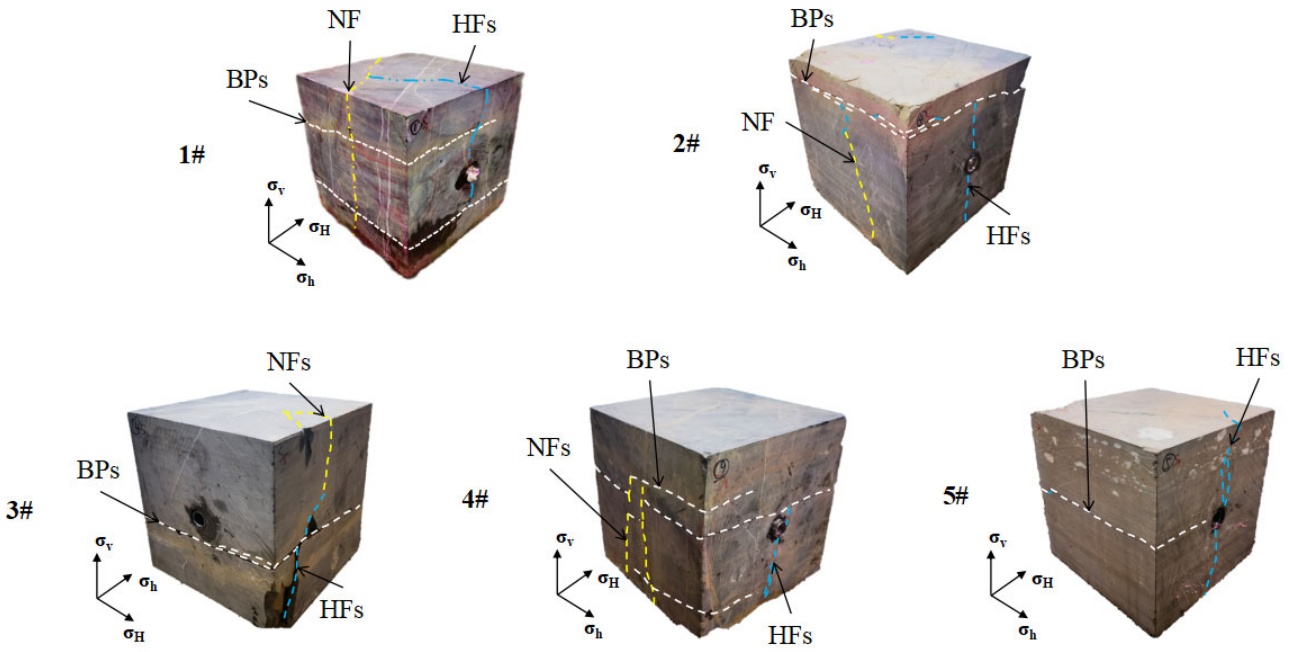


**Figure 4.** Depicts the post-fracture morphology of the five fracturing specimen sets.

Many natural fractures were observed on the surface of specimen 1#. During the conventional sand-carrying fracturing phase, one natural fracture intersecting the horizontal wellbore is initiated (shown by the yellow dashed line), with a fracturing pressure of 7.44 MPa. Subsequently, an in-fracture TPF is conducted, filling and plugging off the natural fracture on the S3 surface with TPA. Two horizontal BPs are opened to the natural fracture (white dashed lines). Finally, in-stage TPF is performed, opening a longitudinal hydraulic fracture near the wellbore (blue dashed line), extending upward through the BPs until reaching the S3 surface, captured by the activated natural fractures, and the BPs intercepts downward extension.

Specimen 2# exhibits significant lithological variations in the upper section, with higher mud content. During the conventional sand-carrying fracturing phase, a longitudinal natural fracture perpendicular to the minimum horizontal principal stress direction is initiated (yellow dashed line), with an inconspicuous fracturing pressure of only 5.00 MPa and insufficient fracture extension. After the in-fracture TPF, the natural fracture deflects and propagates upwards to the high-mud-content area, opening multiple horizontal BPs. In the in-stage TPF, a longitudinal hydraulic fracture is opened near the wellbore, extending upwards to the high-mud-content area and being intercepted by the horizontal BPs.

Specimen 3# has an apparent lithological interlayer below the wellbore. During the conventional sand-carrying fracturing phase, horizontal BPs near the bottom of the wellbore are initiated, with an inconspicuous fracturing pressure peak of only 1.20 MPa. The TPF of the in-fracture effectively plugs the horizontal BPs. A longitudinal hydraulic fracture perpendicular to the minimum horizontal principal stress direction is opened, communicating upwards with the natural fracture and then propagating to the top surface of the specimen, penetrating the heterogeneous lithological interlayer with a high fracturing pressure (15.54 MPa) and large fracture width scale, thus rendering the subsequent in-stage TPF ineffective in initiating fracturing.

Specimen 4# is similar to specimen 1#, with dense natural fractures. During the conventional sand-carrying fracturing phase, significant pressure fluctuations initiate two natural fractures perpendicular to the minimum horizontal principal stress direction and open three horizontal BPs. During the in-fracture TPF phase, a combination of particle-size TPA plugs the natural fractures and BPs, and two longitudinal hydraulic fractures are opened. Two typical shale hydraulic fracture propagation morphologies, namely step-wise diversion and capture by horizontal BPs, are observed on the S5 surface. However, due to wellbore plugs, the in-stage TPF fails to achieve effective fracturing.

Specimen 5# has a high overall mud content with a large and uniformly distributed BP density. During the conventional sand-carrying fracturing phase, a horizontal BP is opened along one side of the wellbore, with a straight and wide fracture width. The TPA is difficult to accumulate during the in-fracture TPF phase, resulting in poor plugging effectiveness. Through in-stage TPF, promoting multi-cluster initiation, the plugging effect is significant, and two longitudinal hydraulic fractures are opened, extending through the BPs to the upper and lower surfaces of the specimen.

## 4. Analysis

### *4.1. The Influence of Different Particle Size Combinations*

Specimens 1#, 2#, and 3# have the same TPA concentration, but different sizes and combination methods were used, resulting in different fracture morphologies and pressure curve characteristics (Figure 5).

As shown in Figure 6, compared with the phase of sand carrying fracturing, different specimens show higher fracture pressure through temporary plugging, and the breakdown pressure under the condition of combined particle size is higher than that under the condition of single particle size at either the phase of temporary plugging in the fracture or the stage. The change trend of breakdown pressure of specimens 1# and 2# is similar. The breakdown pressure of specimen 3# is significantly lower in the phase of sand-carrying fracturing. No large macroscopic fractures are generated, so the effect of in-fracture TPF is more prominent. However, the fractures cannot form effective closure after fracturing, failing subsequent temporary plugging.

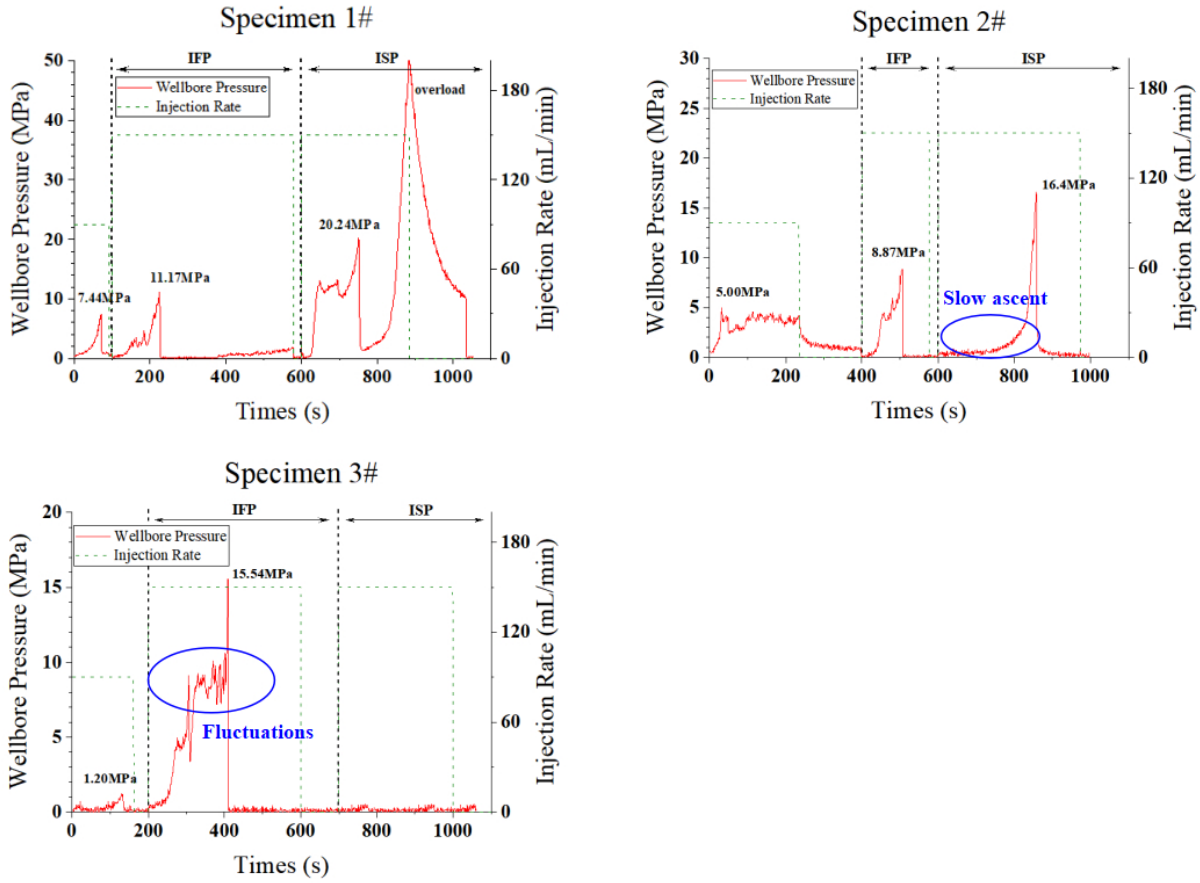


**Figure 5.** The pressure curves of the specimen 1#, 2#, and 3#.

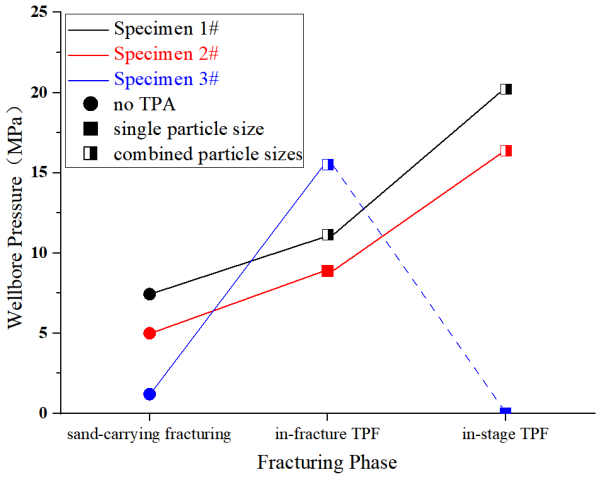


**Figure 6.** Comparison of breakdown/peak pressure in different temporary plugging phases.

During the in-fracture TPF phase, the breakdown pressures of specimens 1# and 3# (11.17 MPa and 15.54 MPa, respectively) increased by 25.9% and 75.2%, respectively, compared to specimen 2# (8.87 MPa). During the in-fracture temporary plugging phase, specimens 1# and 2# exhibited significant breakdown pressures of 20.24 MPa and 16.4 MPa, respectively, while specimen 3# failed to plug effectively. Compared to the single particle size plugging method, combining different particle sizes of TPA, with large particles bridging and small particles plugging the gaps between large particles, is conducive to improving plugging efficiency.

In contrast to specimen 1#, specimen 3# used a higher proportion of small-particle (80–120 mesh) TPAs during the in-fracture TPF phase, resulting in more pronounced pressure curve fluctuations and a slower establishment of pressure balance. However, the final breakdown pressure was higher, with the tiny particles entering the fractures for complete plugging. Compared to specimen 1#, specimen 2# had a richer combination of TPA sizes during the in-stage TPF phase, with higher proportions of medium (20–80 mesh) and small (80–120 mesh) particle sizes. However, the breakdown pressure was lower, and its pressure curve experienced a longer period of slow rise during the early time of in-stage TPF (Figure 5). This indicates that a larger-particle-size TPA should be prioritized to bridge larger-sized fractures to prevent the loss of smaller TPAs into the fractures.

### *4.2. The Impact of Different Concentrations*

Specimens 1#, 4#, and 5# used the same types and combination methods of TPA sizes but with different concentrations of 100 g/L, 80 g/L, and 60 g/L, respectively.

During the in-fracture TPF phase, at a TPA concentration of 60 g/L (Specimen 5#), the pressure fluctuated, making effective plugging difficult, with no significant breakdown pressure and a peak pressure of only 4.44 MPa (Figure 7). When the TPA concentration was increased to 80 g/L (Specimen 4#), the peak pressure rose to 10.63 MPa, with apparent breakdown pressure and a significant plugging effect. Further increasing the concentration to 100 g/L (Specimen 1#), the peak pressure reached its maximum at 11.17 MPa. Although the pressure increase was insignificant, the slope of the pressure curve was steeper (Figure 8), indicating a faster pressure response and plugging.

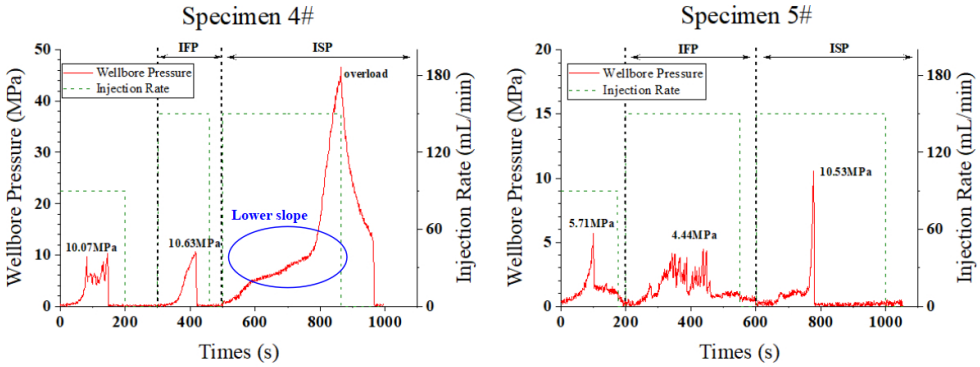


**Figure 7.** The pressure curves of specimens 4# and 5#.

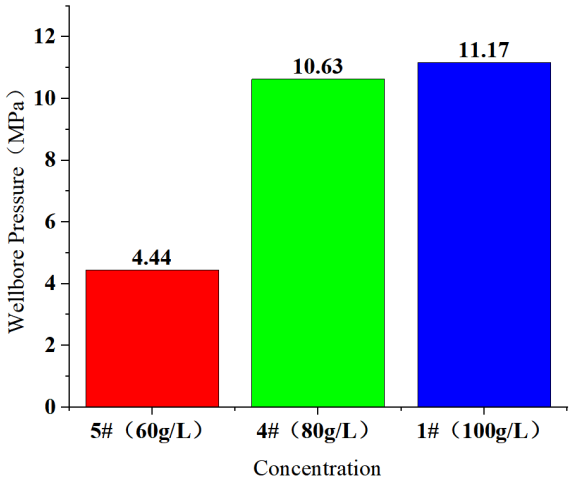


**Figure 8.** The wellhead pressure during in-fracture temporary plugging under different plugging agent concentrations.

During the in-stage TPF phase, as the concentration of the TPA increased from 60 g/L (Specimen 5#) to 80 g/L (Specimen 4#) and 100 g/L (Specimen 1#), the pressure significantly increased (Figure 9), surpassing the safety limit of the equipment. Effective breakdown pressure could not be monitored. However, compared to the condition of 80 g/L (Specimen 4#), the upward slope of the pressure curve for 100 g/L (Specimen 1#) was steeper, indicating a more rapid and effective plugging process.

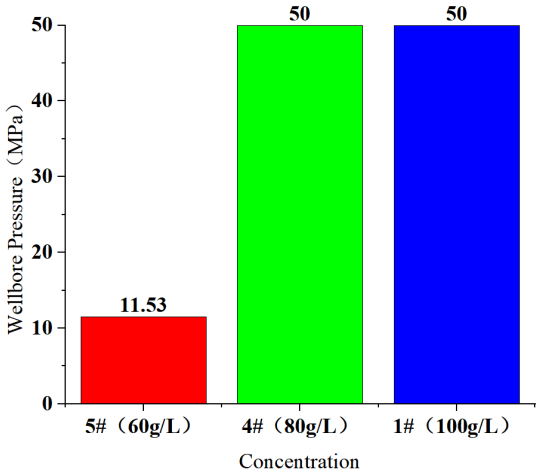


**Figure 9.** The wellhead pressure during the in-stage TPF under different TPA concentrations.

## 5. Discussion

Specimens 1# and 4# exhibit lots of natural fractures by contrasting the different lithological characteristics of specimens. Following the experiment, horizontal BPs near the wellbore were initiated and communicated with the natural fractures. Longitudinal hydraulic fractures were formed through TPF measures (shown in Figures 10 and 11d). Specimen 2# contains regions with high mud-content lithological variations, forming simple longitudinal hydraulic fractures extending to the high mud-content areas and activating horizontal BPs (shown in Figures 10 and 11a). Specimen 3# displays distinct heterogeneous lithological interlayers. Conventional sand-carrying hydraulic fractures struggle to penetrate these interlayers, thus enhancing the initiation pressure through TPF to facilitate fracture penetration and propagation (shown in Figures 10 and 11b). Specimen 5# exhibits high mud content and high BP density. Conventional sand-carrying fracturing and in-fracture TPF demonstrate poor effectiveness. However, in-stage TPF generates relatively singular longitudinal hydraulic fractures (shown in Figures 10 and 11c).

Therefore, we can infer that in the field fracturing process, for shale reservoirs, typically characterized by BPs of varying densities, horizontal BPs near the wellbore are prone to open during conventional proppant fracturing phases with low fracture pressures, making it difficult to propagate across layers and form complex fracture networks. However, employing TPA with different concentrations and particle size combinations can effectively increase the fracturing pressure, enhance the vertical communication capability of artificial fractures, and significantly enhance the complexity of fracture morphology. Target stratum with lower BP densities would show an improvement in fracture pressure to a certain extent during in-fracture and in-stage TPF phases, achieving fracture redirection and forming complex fracture networks. On the other hand, the target stratum with higher BP densities tends to open BPs near the wellbore, exhibiting poor performance in in-fracture TPF. In contrast, in-stage TPF is more conducive to forming interlayer fractures, thereby achieving reservoir stimulation effects.

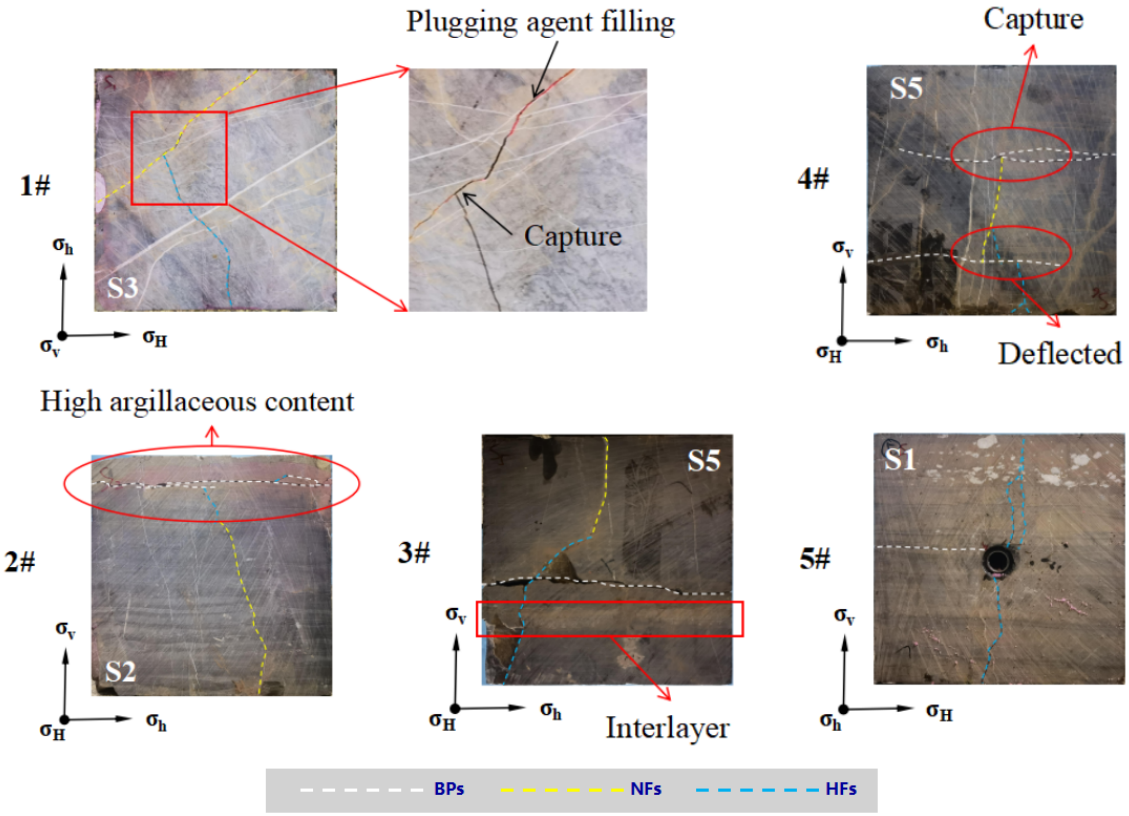


**Figure 10.** Fracture morphology of specimens with different lithology characteristics.

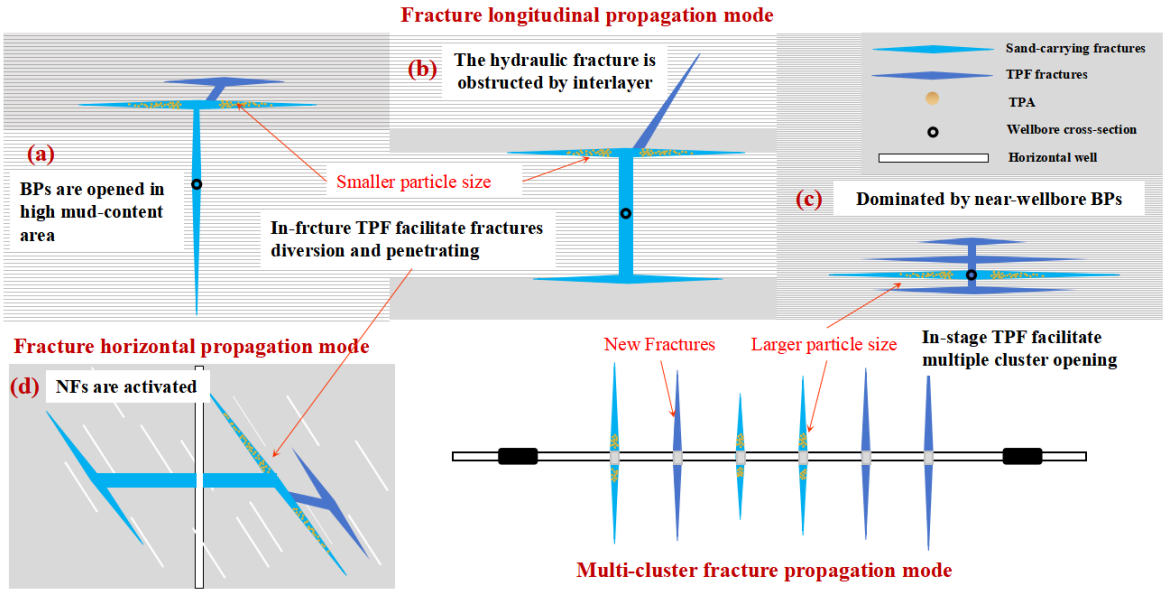


**Figure 11.** Different fracture propagation modes.

## 6. Conclusions

By conducting TPF experiments with different particle size combinations and concentrations of TPA at both in-fracture and in-stage locations, combined with the morphology of the fracturing fractures and the characteristics of pressure curves, the influence of different TPA parameters on TPF effectiveness was analyzed. The results indicate the following:

1. Combined particle sizes can enhance plugging effectiveness, combining smaller and larger particles, resulting in higher breakdown pressures and better plugging effects.

However, merely increasing the combination types of temporary plugging agent particle sizes does not necessarily yield better temporary plugging effects. By comparing the pressure curves during in-stage TPF of specimens 1# and 2#, it is evident that increasing the proportion of larger particles can better exploit the bridging effect of the plugging agent, thereby avoiding the loss of smaller particle plugging agents.

2. Higher concentrations of TPA lead to more pronounced TPF breakdown pressures, facilitating the formation of multiple, wider diversion fractures, thereby achieving significant plugging effects. During the in-fracture TPF phase, the TPA sizes in the experimental design are relatively small, allowing hydraulic fractures to provide ample migration and filling space for the TPA. However, during the in-stage plugging phase, the migration space for the plugging agent is limited, resulting in two groups of wellbore plugs (1# and 4#). Therefore, in actual field TPF operations, the upper limit of plugging agent concentration should be considered more carefully.
3. For shale reservoirs with high density of BPs, specimens with relatively lower BP density exhibit good performance in both in-fracture and in-stage TPF, forming complex fracture networks. Conversely, specimens with higher BP density perform better in-stage than in-fracture TPF.

**Author Contributions:** Conceptualization, F.Y.; methodology, Q.Q.; validation, M.L.; formal analysis, W.H.; investigation, A.Z.; resources, Z.Z.; data curation, Y.Z.; writing—original draft preparation, D.Z.; writing—review and editing, Y.Z.; visualization, D.Z.; supervision, Y.Z.; project administration, F.Y.; funding acquisition, F.Y. All authors have read and agreed to the published version of the manuscript.

**Funding:** This research was funded by China Postdoctoral Science Foundation, grant number 2021M702304 and Shandong Provincial Natural Science Foundation, grant number ZR2021QE260.

**Data Availability Statement:** Data available on request due to restrictions, e.g., privacy or ethical: The data presented in this study are available on request from the corresponding author. The data are not publicly available due to [Some data and materials originate from the oilfield site and are required to be kept confidential in accordance with local laws and regulations].

**Conflicts of Interest:** Authors Feng Yang, Qin Qian, Mingjing Lu, Wenjun He, Anhai Zhong and Zilin Zhang were employed by the Sinopec Shengli Oilfield Company. The remaining authors declare that the research was conducted in the absence of any commercial or financial relationships that could be construed as a potential conflict of interest. The Sinopec Shengli Oilfield Company had no role in the design of the study; in the collection, analyses, or interpretation of data; in the writing of the manuscript, or in the decision to publish the results.

## Nomenclature

| | |
|---|---|
| TPF | temporary plugging fracturing |
| TPA | temporary plugging agent |
| BPs | bedding planes |
| $S$ | clusters' spacing |
| $L$ | width of the treatment zone |
| $\beta$ | empirical parameter |
| $\mu$ | viscosity |
| $t$ | fracture propagation time |
| $Q$ | injection rate |
| $E$ | elastic modulus of rock |
| $E'$ | plane strain elastic modulus |
| $K'$ | modified fracture toughness |
| $R$ | fracture propagation radius |
| $\sigma_{\mathrm{H}}$ | maximum horizontal principal stress |
| $\sigma_h$ | minimum horizontal principal stress |
| $\sigma_v$ | vertical stress |
| Subscript: | |
| $l$ | experimental parameters |
| $f$ | field parameters |

## References


1. Shahri, M.P.; Huang, J.; Smith, C.S.; Fragachán, F.E. An Engineered Approach to Design Biodegradables Solid Particulate Diverters: Jamming and Plugging. In Proceedings of the SPE Annual Technical Conference and Exhibition, San Antonio, TX, USA, 10 October 2017; OnePetro: Richardson, TX, USA, 2017.
2. Xue, S.; Zhang, Z.; Wu, G.; Wang, Y.; Wu, J.; Xu, J. Application of a Novel Temporary Blocking Agent in Refracturing. In Proceedings of the SPE Asia Pacific Unconventional Resources Conference and Exhibition, Brisbane, Australia, 9–11 November 2015; OnePetro: Richardson, TX, USA, 2015.
3. Abrams, A. Mud Design to Minimize Rock Impairment Due to Particle Invasion. *J. Pet. Technol.* **1977**, *29*, 586–592. [CrossRef]
4. Dick, M.A.; Heinz, T.J.; Svoboda, C.F.; Aston, M. Optimizing the Selection of Bridging Particles for Reservoir Drilling Fluids. In Proceedings of the SPE International Symposium on Formation Damage Control, Lafayette, LA, USA, 23–24 February 2000.
5. Van Domelen, M.S. A Practical Guide to Modern Diversion Technology. In Proceedings of the SPE Oklahoma City Oil and Gas Symposium, Oklahoma City, OK, USA, 27–31 March 2017; OnePetro: Richardson, TX, USA, 2017.
6. Weddle, P.; Griffin, L.; Pearson, C.M. Mining the Bakken: Driving Cluster Efficiency Higher Using Particulate Diverters. In Proceedings of the SPE Hydraulic Fracturing Technology Conference and Exhibition, The Woodlands, TX, USA, 26 January 2017; OnePetro: Richardson, TX, USA, 2017.
7. Gomaa, A.M.; Nino-Penaloza, A.; Castillo, D.; McCartney, E.; Mayor, J. Experimental Investigation of Particulate Diverter Used to Enhance Fracture Complexity. In Proceedings of the SPE International Conference and Exhibition on Formation Damage Control, Lafayette, LA, USA, 24–26 February 2016; OnePetro: Richardson, TX, USA, 2016.
8. Zhu, D.; Xu, Z.; Sun, R.; Fang, X.; Gao, D.; Jia, X.; Hu, J.; Weng, J. Laboratory Evaluation on Temporary Plugging Performance of Degradable Preformed Particle Gels (DPPGs). *Fuel* **2021**, *289*, 119743. [CrossRef]
9. Yang, C.; Zhou, F.; Feng, W.; Tian, Z.; Yuan, L.; Gao, L. Plugging Mechanism of Fibers and Particulates in Hydraulic Fracture. *J. Pet. Sci. Eng.* **2019**, *176*, 396–402. [CrossRef]
10. Fan, F.; Zhou, F.; Yuan, L.; Yang, X. Visualization Study on Plugging Mechanism of Fibers and Particles in Rough and Tortuous Fracture. In *Proceedings of the Volume 8: Polar and Arctic Sciences and Technology*; Petroleum Technology: Glasgow, UK, 2019.
11. Zhang, R.; Hou, B.; Tan, P.; Muhadasi, Y.; Fu, W.; Dong, X.; Chen, M. Hydraulic Fracture Propagation Behavior and Diversion Characteristic in Shale Formation by Temporary Plugging Fracturing. *J. Pet. Sci. Eng.* **2020**, *190*, 107063. [CrossRef]
12. Zhang, W.; Shi, X.; Jiang, S.; Cao, Q.; Wang, F.; Wang, Z.; Ge, Y.; Du, Y. Experimental Study of Hydraulic Fracture Initiation and Propagation in Highly Saturated Methane-Hydrate-Bearing Sands. *J. Nat. Gas Sci. Eng.* **2020**, *79*, 103338. [CrossRef]
13. Wang, B.; Zhou, F.; Yang, C.; Xu, C.; Liu, J.; Han, S.; Wang, D.; Ren, Z.; Liang, T. A Novel Experimental Method to Investigate the Plugging Characteristics of Diversion Agents within Hydro-Fracture. *J. Pet. Sci. Eng.* **2019**, *183*, 106354. [CrossRef]
14. Wang, B.; Zhou, F.; Yang, C.; Wang, D.; Yang, K.; Liang, T. Experimental Study on Injection Pressure Response and Fracture Geometry during Temporary Plugging and Diverting Fracturing. *SPE J.* **2020**, *25*, 573–586. [CrossRef]
15. Potapenko, D.I.; Tinkham, S.K.; Lecerf, B.; Fredd, C.N.; Samuelson, M.L.; Gillard, M.R.; Le Calvez, J.H.; Daniels, J.L. Barnett Shale Refracture Stimulations Using a Novel Diversion Technique. In Proceedings of the SPE Hydraulic Fracturing Technology Conference, The Woodlands, TX, USA, 19–21 January 2009; OnePetro: Richardson, TX, USA, 2009.
16. Carpenter, C. A Novel Completion Method for Sequenced Fracturing in the Eagle Ford Shale. *J. Pet. Technol.* **2014**, *66*, 122–125. [CrossRef]
17. Gomaa, A.M.; Sun, H.; Nelson, S.; Qu, Q.; Boncan, G.V. Using Swelling Materials to Control Fracture Complexity: Experimental Study. In Proceedings of the SPE Annual Technical Conference and Exhibition, Houston, TX, USA, 28–30 September 2015; OnePetro: Richardson, TX, USA, 2015.
18. Ma, X.; Zou, Y.; Li, N.; Chen, M.; Zhang, Y.; Liu, Z. Experimental Study on the Mechanism of Hydraulic Fracture Growth in a Glutenite Reservoir. *J. Struct. Geol.* **2017**, *97*, 37–47. [CrossRef]
19. Bunger, A.P.; Jeffrey, R.G.; Detournay, E. Application of Scaling Laws to Laboratory-Scale Hydraulic Fractures. In Proceedings of the Alaska Rocks 2005, The 40th U.S. Symposium on Rock Mechanics (USRMS), Anchorage, AK, USA, 25–29 June 2005; OnePetro: Richardson, TX, USA, 2005.
20. Detournay, E. Mechanics of Hydraulic Fractures. *Annu. Rev. Fluid Mech.* **2016**, *48*, 311–339. [CrossRef]
21. Dontsov, E.V. An Approximate Solution for a Plane Strain Hydraulic Fracture That Accounts for Fracture Toughness, Fluid Viscosity, and Leak-Off. *Int. J. Fract.* **2017**, *205*, 221–237. [CrossRef]
22. Madyarov, A.; Prioul, R.; Zutshi, A.; Seprodi, N.; Groves, D.; Pei, J.; Wong, S.-W. Understanding the Impact of Completion Designs on Multi-Stage Fracturing via Block Test Experiments. In Proceedings of the 55th U.S. Rock Mechanics/Geomechanics Symposium, Virtual, 18–25 June 2021; OnePetro: Richardson, TX, USA, 2021.